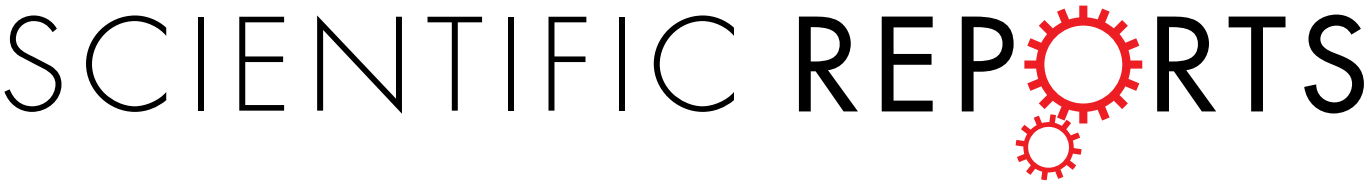

OPEN

Received: 06 September 2015
Accepted: 04 January 2016
Published: 16 February 2016

Enhancing the energy density of safer Li-ion batteries by combining high-voltage lithium cobalt fluorophosphate cathodes and nanostructured titania anodes

Gregorio F. Ortiz[1], María C. López[1], Yixiao Li[2], Matthew J. McDonald[2], Marta Cabello[1], José L. Tirado[1] & Yong Yang[2]

Recently, Li-ion batteries have been heavily scrutinized because of the apparent incompatibility between safety and high energy density. This work report a high voltage full battery made with TiO_2/Li_3PO_4/Li_2CoPO_4F. The Li_2CoPO_4F cathode and TiO_2 anode materials are synthesized by a sol–gel and anodization methods, respectively. X-ray diffraction (XRD) analysis confirmed that Li_2CoPO_4F is well-crystallized in orthorhombic crystal structure with *Pnma* space group. The Li_3PO_4-coated anode was successfully deposited as shown by the (011) lattice fringes of anatase TiO_2 and (200) of γ-Li_3PO_4, as detected by HRTEM. The charge profile of Li_2CoPO_4F versus lithium shows a plateau at 5.0V, revealing its importance as potentially high-voltage cathode and could perfectly fit with the plateau of anatase anode (1.8–1.9V). The full cell made with TiO_2/Li_3PO_4/Li_2CoPO_4F delivered an initial reversible capacity of 150 mA h g^{-1} at C rate with good cyclic performance at an average potential of 3.1–3.2V. Thus, the full cell provides an energy density of 472 W h kg^{-1}. This full battery behaves better than TiO_2/Li_2CoPO_4F. The introduction of Li_3PO_4 as buffer layer is expected to help the cyclability of the electrodes as it allows a rapid Li-ion transport.

Li-ion technology is now mature enough to meet the exacting demands of portable electronic devices and even electric vehicles. However, recently Li-ion batteries (LIBs) have come under heavy scrutiny because of an apparent incompatibility between safety and high energy density. The capabilities of LIBs are governed by the chemistry of the cathode, which almost exclusively utilizes transition metal insertion/intercalation reactions. The cathode material is not only the most expensive part of the battery but also the primary limitation on the electrochemical performance. It is thus desirable to find high voltage cathode materials with high capacity (xLi $\gg$ 1) and good electrolyte stability. $LiNi_{0.5}Mn_{1.5}O_4$ spinel, $LiCoPO_4$ olivine, $LiNiVO_4$ inverse spinel and Li_2CoPO_4F fluorophosphates are currently considered to be the most promising 5-V cathode voltage materials available[1–6]. On the other side of the battery, there are a large number of possibilities for anodes to be combined with cathodes, but some of the most outstanding anodes with respect to safety performance are $Li_4Ti_5O_{12}$ and TiO_2, which can replace carbonaceous materials[7–10]. The TiO_2 electrodes vs. Li_2CoPO_4F can be considered safer than other Li-ion systems based on carbon anodes, due to the higher working voltage of the anode that avoids lithium electrodeposition, which is well known to jeopardize safety, while energy density is preserved or even improved by the use of the high-voltage cathode.

Up until now, one of the more impressive LIB electrochemical performances has been seen in the $Li_4Ti_5O_{12}$/Li_2CoPO_4F, primarily because it exhibits a voltage plateau at about 3.4 V which is higher than that of a $Li_4Ti_5O_{12}$/$LiFePO_4$ full cell at ~1.9 V[11,12]. However, an unresolved problem with the former system is that capacity decays abruptly in the first few cycles, and as of yet no improvement in cycling performance has been achieved. As far

[1]Inorganic Chemistry Laboratory, University of Córdoba, Marie Curie Building, Campus of Rabanales, E-14071 Córdoba, Spain. [2]State Key Laboratory of Physical Chemistry of Solid Surfaces, Department of Chemistry, College of Chemistry and Chemical Engineering, Xiamen University, Xiamen 361005, P. R. China. Correspondence and requests for materials should be addressed to G.F.O. (email: q72maorg@uco.es)

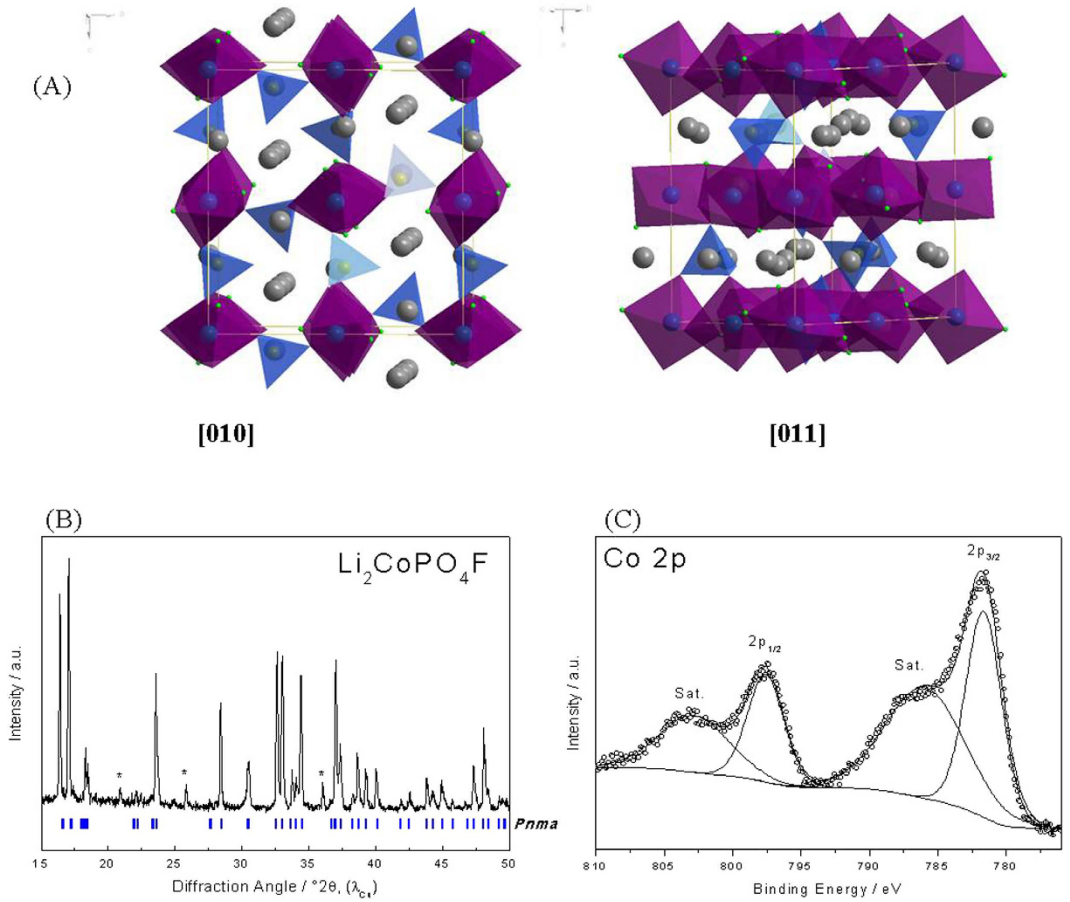

Figure 1. (**A**) Schematic view of the crystal structure of Li_2CoPO_4F along the [010] and [011] directions. (**B**) XRD pattern, and (**C**) XPS of the Co2p area from a Li_2CoPO_4F sample.

as we know, there are no reports in the literature dealing with TiO_2/Li_2CoPO_4F that can reach theoretical energy densities above 450 W h kg^{-1}, performance close to the demands of modern applications.

In order to improve the cyclability of high voltage LIBs, the effects of a surface treatment of lithium phosphate on a full cell made with Li_2CoPO_4F as cathode and TiO_2 as anode were studied. This report shows how the electrochemical performance of this material compared very favourably with Li_3PO_4-free electrodes. The introduction of an inactive matrix such as Li_3PO_4 for use as a buffer layer is expected to help the cyclability of the electrodes by allowing a rapid transportation of Li ions[13,14].

Results and Discussion

Figure 1A shows a schematic view of the Li_2CoPO_4F structure. It is formed by chains of CoO_4F_2 octahedra sharing their edges and interconnected with PO_4 tetrahedral oxo-anions by corner sharing. The solid possesses an orthorhombic unit cell with *Pnma* space group, where there are 3 types of Li; Li1 in 8d sites and Li2 and Li3 in two sets of 4c sites. The Co is in 4a and 4b sites, the P in two sets of 4c sites, the F in two sets of 4c sites, and the O in four sets of 4c and two sets of 8d sites[6]. The cross linked structure forms an opened 3D framework, permitting Li ions to be inserted and extracted from multiple directions[15–17]. The XRD pattern of the synthesized Li_2CoPO_4F sample shown in Fig. 1B shows diffraction peaks indexed in agreement with the literature values, with a = 10.452 Å, b = 6.3911 Å, and c = 10.874 Å[6,17]. A $LiCoPO_4$ impurity phase was detected (marked with symbol * in Fig. 1B), which could have been due to the relatively low heat treatment temperature[11,15]. The XPS signal of the Co2p, split into the $2p_{3/2}$ and $2p_{1/2}$ multiplet separated by 15.7 eV, is formed by a double peak at 781.7 eV and 786.2 eV (Fig. 1C), assigned to the Co^{2+}in Li_2CoPO_4F in very good agreement with the observation reported in ref. 15.

The Li_3PO_4-coated TiO_2 anode was prepared at room temperature, with some material also annealed at 500 °C in air for 2 h. The XRD patterns of the materials exhibit different features (Fig. 2). While for the as-prepared specimen, only Ti reflections (JCPDS file 05–0682 and space group $P6_3/mmc$) can be observed, the annealed sample shows very intense peaks of anatase (JCPDS 21-1272 and space group $I4_1/amd$). In both cases the presence of Li_3PO_4 could not be detected by XRD, due to the low crystallinity and small amounts of solid controlled by the conditions of the electrolytic deposition. Since the Li_3PO_4 is on the surface of TiO_2 nanotubes further experiments allowed us to detected the (110), (101), (210) and (002) reflections of β-Li_3PO_4 (JCPDS 25–1030) phase for large time (20 min) and high current density (75 mA cm^{-2}) during electrolytic deposition[13]. Previous experiments conducted to synthesize thick layers of lithium phosphate covering the complete surface of titania

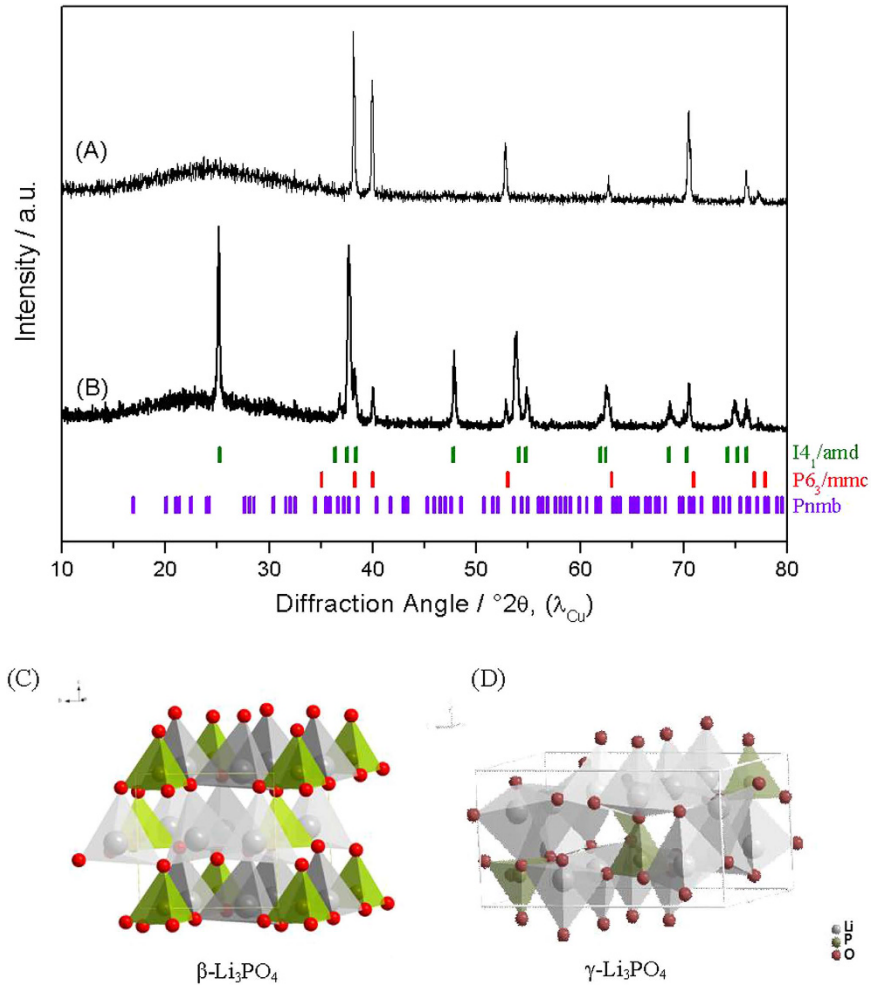

Figure 2. XRD patterns of Li_3PO_4-coated TiO_2 anode (**A**) as-prepared and (**B**) after thermal annealing at 500 °C in air for 2 h. (**C,D**) show representations of the crystal structure of β-Li_3PO_4 and γ-Li_3PO_4, respectively.

nanotubes[13]. So, this over 20 μm thick layer would passivate the active electrode and cannot be beneficial for such cycling purposes as electrodes in batteries. For this reason, we scaled down the fabrication of Li_3PO_4 layer to the nanometric size, observing that the best ratio of Li_3PO_4 to TiO_2 is $9.03{\cdot}10^{-3}$ g Li_3PO_4/g TiO_2. By using optimal current densities and deposition times of ca. – 3.75 mA cm^{-2} and 1 min a finely dispersed layer of Li_3PO_4 can fill the titania nanotubes (see Supplementary Fig. S1 online). Under these conditions no diffraction peaks either of β-Li_3PO_4 or γ-Li_3PO_4 were detected in the X-ray diffraction patterns which were recorded from 10–80° (°2θ) with 0.02° of step size each 2 seconds as discussed above. Having a detailed inspection with HRTEM and SAED, the formation of β-Li_3PO_4 (at room temperature) or γ-Li_3PO_4 (when annealing) on titania nanotubes was unveiled as discussed below.

The lithium phosphate seems to play an important role enhancing the electrochemical response, both in Li half cells and in full Li-ion batteries, and deserves to be studied in more detail[13,17–19]. The β-Li_3PO_4 has a basic wurtzite structure where one position of the tetrahedral sites, T+ or T−, is fully occupied, along with cation ordering (Fig. 2C). It has twice the value of the unit cell along the axis when the phase transition from β- to γ-Li_3PO_4 (Fig. 2D) occurs. The γ-phase also consists of hexagonal close-packed oxide layers, but these are more distorted in comparison with the β-structure. Moreover, the cations are distributed over both sets of T+ and T− sites, leading LiO_4 tetrahedra to share some of their edges, while only corner-sharing is present in the β-structure[20–22].

In order to examine the formation of phosphate phases on titania nanotubes and discover whether or not an additional phase is formed at the interface, HRTEM and SAED measurements were performed. The HRTEM image of the "AD" sample (which was not calcined) is shown in Fig. 3A, which shows areas having visible lattice fringes measured and labelled according to their particular crystal structures. It can be seen that β-Li_3PO_4 was successfully formed, with the image containing a small region of ordered crystalline structure with a (110) interplanar spacing of 0.399 nm[23]. Here, amorphous TiO_2 was not detected, but fringes corresponding to the (222) reflection of $Li_4Ti_5O_{12}$ with an interplanar spacing of 0.245 nm were found[24]. This image was taken at the tip of the nanotube and we can observe that lithium titanate appeared at both sides of the region of lithium phosphate, which could explain the lack of TiO_2 detection. The SAED data in Fig. 3B matches these d-spacings and confirms the presence of these materials. Figure 3C shows HRTEM imagery of the ADC sample (which was calcined), with regions of visible lattice fringes measured and labeled to identify their respective crystal structures. Here, a small

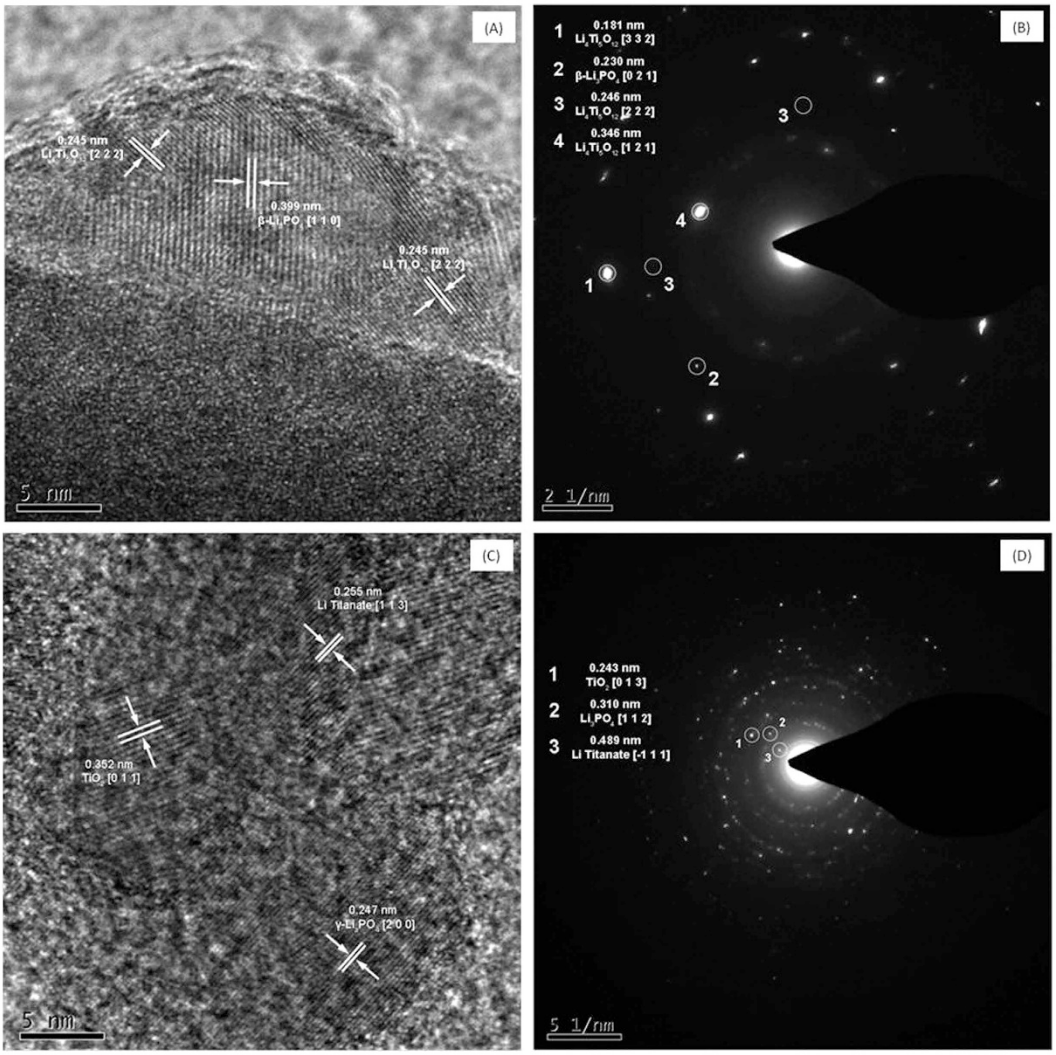

Figure 3. HRTEM and SAED imagery of (**A,B**) AD and (**C,D**) ADC samples, respectively.

region showing an ordered crystalline structure with a (011) interplanar spacing of 0.352 nm was detected, corresponding to anatase TiO_2[25]. However, the observed form of lithium phosphate was γ-Li_3PO_4 as deduced from the (200) reflection ($d_{200} = 0.247$ nm), as expected after thermal annealing at 500 °C[26]. In addition, fringes corresponding to lithium titanate are also visible ($d_{113} = 0.255$ nm)[24]. The anatase TiO_2, γ-Li_3PO_4 and $Li_4Ti_5O_{12}$ regions are labeled "1", "2" and "3" respectively to avoid confusion. The SAED data in Fig. 3D shows fine diffraction points corresponding to these three phases. The presence of small amounts of the $Li_4Ti_5O_{12}$ phase at the interface between Li_3PO_4 and TiO_2 gives an additional understanding of the structure of these composites.

The cathode half-cell reaction can be written as:

$$Li_2CoPO_4F \leftrightarrows Li_{2-x}CoPO_4F + xLi^+ + xe^- \quad (1)$$

The theoretical capacity of Li_2CoPO_4F is 287 mA h g^{-1} for x = 2. However, recent studies have indicated that Li_2CoPO_4F can reach a maximum reversible capacity of 150 mA h g^{-1}, with an outstanding high-voltage operation of ~5 V vs. Li^+/Li[11,15,27–30]. Because of the high inefficiency from the first to the second cycle observable in Li_2CoPO_4F, these electrodes were subjected to activation cycles before being used in the complete lithium-ion cell (see Supplementary Fig. S2 online). The first-cycle irreversible capacity due to electrolyte decomposition was then avoided in the full cells[11,15]. Anatase is well known in the literature to exhibit a high reversibility in the first cycle and to operate at a safe average potential of 1.8–1.9 V vs. Li^+/Li. The theoretical capacity delivered by anatase is around 167 mA h g^{-1} according to the following reaction:

$$nt\text{–}TiO_2 + 0.5Li^+ + 0.5e^- \leftrightarrows nt\text{–}Li_{0.5}TiO_2 \quad (2)$$

Taking into account their individual voltages, the combination of nt-TiO_2 with Li_2CoPO_4F could give rise to a battery operating in the 3.1–3.2 V range. While considering the expected capacity of each electrode, the main overall reaction that may take place in the full cells can be summarized as follows:

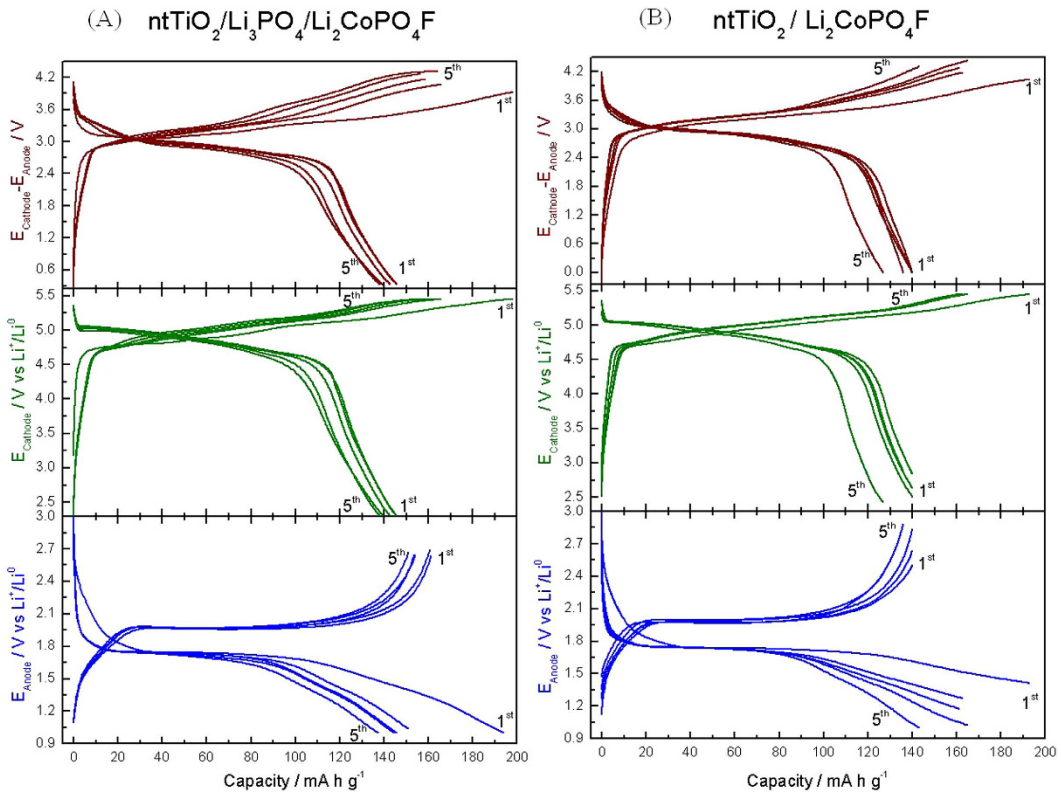

Figure 4. Galvanostatic charge/discharge cycles representing the $E_{Cathode} - E_{Anode}$ vs. capacity of (**A**) nt-TiO_2/γ-Li_3PO_4/Li_2CoPO_4F, and (**B**) nt-TiO_2/Li_2CoPO_4F cells. This figure includes the voltage profiles of the cathode ($E_{Cathode}$ vs. capacity) and the anode (E_{Anode} vs. capacity) in the middle and bottom plots. The capacity of the full cell is calculated using the cathode mass.

$$1/2Li_2CoPO_4F + nt\text{–}TiO_2 \leftrightarrows 1/2LiCoPO_4F + nt\text{–}Li_{0.5}TiO_2 \quad (3)$$

Capacity balance was carried out by assuming 140 mA h g^{-1} reversible capacity of the cathode after activation and 160 mA h g^{-1} of the anode (see Fig. 4), the resulting cathode mass to anode mass was: m+/m− = 1.14.

Figure 4A,B compare the reversible voltage profile versus Li of the TiO_2 with and without Li_3PO_4 (bottom) and of the Li_2CoPO_4F cathode (middle). The anode operates reversibly with continuous, plateaued charge-discharge curves with a reversible capacity of 150 mA h g^{-1} at an average voltage value of about 1.8–1.9 V, while the Li_2CoPO_4F cathode cycles with a reversible capacity of 148 mA h g^{-1} at a voltage value of 5 V vs. Li with a flat plateau, typical of the two phase reaction of lithium-cobalt fluorophosphates[19].

The upper plots of Fig. 4A,B show the trend of the full-cell voltage profile, demonstrating very stable behaviour. The cell operates with an average voltage of around 3.1–3.2 V, while the voltage profile is the combination of the flat voltage of the Li_2CoPO_4F cathode (Fig. 4 middle plots) and the flat voltage of the TiO_2 (Fig. 4B bottom plot) or TiO_2/γ-Li_3PO_4 anodes (Fig. 4A bottom plot). The reversible capacity of the full battery measured at a state of discharge is about 150 mA h g^{-1}, reaching about 99% of the maximum reversible capacity. The achieved energy density is 472 W h kg^{-1}, an enhanced value as compared to the majority of published batteries[31–36].

$Li_4Ti_5O_{12}$ is a well-known material for LIBs and typically shows a stable plateau at 1.54 V (vs. Li^+/Li)[7,37–39]. However, such a plateau is not visible in the charge/discharge curves (Fig. 4A,B bottom plots). Instead, the typical plateau of anatase TiO_2 can be seen. The lithium titanate phase is formed in a minute fraction at the interphase between TiO_2 and Li_3PO_4, as detected by SAED and HRTEM measurements (Fig. 3). However, this phase was not detected by XRD (Fig. 2), due to its particularly low proportion. Then, its contribution to battery functionality is expected to be negligible.

The stability of chosen electrode materials is another key factor for battery cycling. Figure 5 compares the cycling stability of TiO_2/Li_3PO_4/Li_2CoPO_4F and TiO_2/Li_2CoPO_4F measured at 1 C, 2 C and 5 C rates. The battery that utilizes Li_3PO_4 shows very good cycling behaviour as compared to that of the full cell without Li_3PO_4, operating at 1 C, 2 C and 5 C rates for more than 240 charge-discharge cycles with high coulombic efficiencies of 79, 62 and 73%, respectively. These differences were found significant from a statistical analysis of cycling experiments of five different cells for each composition that can be found as Supplementary Table S1 online. As expected, capacity decay from 150 mA h g^{-1} at 1 C to 120 mA h g^{-1} is recorded at 2 C, and to 90 mA h g^{-1} at 5 C. This battery, based on TiO_2/Li_3PO_4/Li_2CoPO_4F, exhibits much better performance in terms of cyclability and coulombic efficiency than TiO_2/Li_2CoPO_4F and that previously reported and based on $Li_4Ti_5O_{12}$ as an anode material[11]. The excellent performance of this battery observed in terms of specific capacity, cycling life and rate capability is to the best of

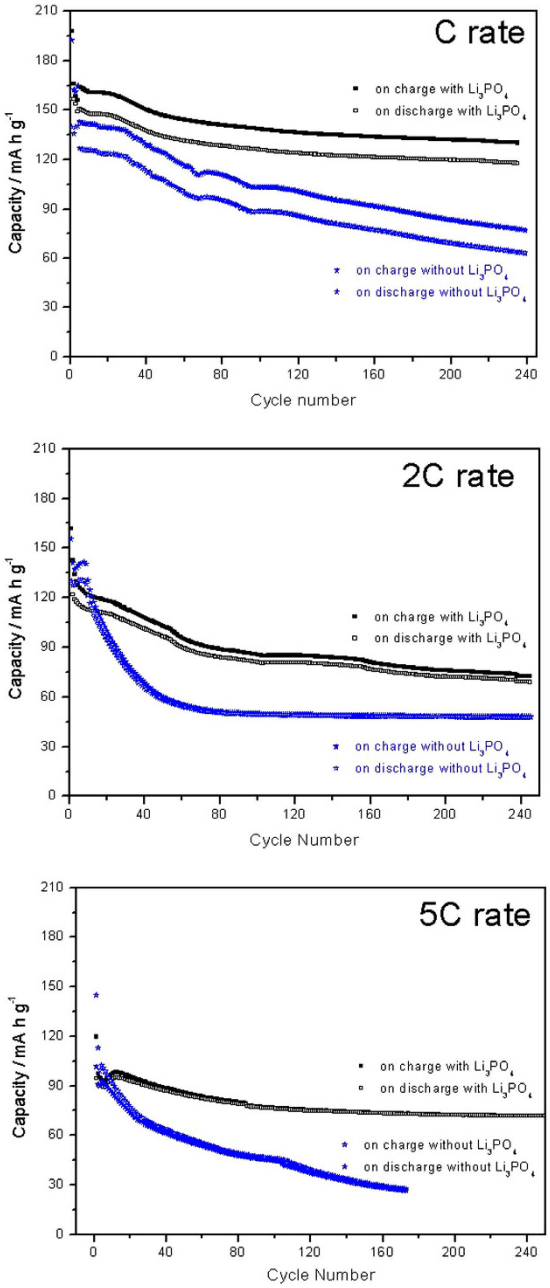

Figure 5. A comparison of specific capacity versus cycle number between nt-TiO_2/Li_2CoPO_4F, and nt-TiO_2/γ-Li_3PO_4/Li_2CoPO_4F cells, calculated at 1 C, 2 C, and 5 C rates.

our knowledge only seldom reported, and confirms the great potential of TiO_2/Li_3PO_4 as an innovative electrode material that can aid the progress of lithium-based energy storage systems.

Conclusions

The high working voltage and excellent rate capability observed of the TiO_2/Li_3PO_4/Li_2CoPO_4F full cell makes it a promising high energy density LIB with acceptable rate performance (472 W h kg^{-1} at a 1 C rate, and 284 W h kg^{-1} at a 5 C rate), preventing the emergence of safety issues caused by the highly reactive lithiated graphite present in most LIB systems. The existence of Li_3PO_4 and the minute fraction of $Li_4Ti_5O_{12}$ present between the TiO_2/Li_3PO_4 interfaces can explain the good cyclability of the full cell as this inactive matrix allows rapid transportation of the lithium ions.

Methods

The Li_2CoPO_4F/C nanocomposite was synthesized by the sol-gel (SG) method as previously reported[11,15]. The self-organized titania nanotube (nt–TiO_2) layer was fabricated by an anodization process using Ti foils at 60 V for 2 h, with a freshly prepared mixture of EG/water (92:8 vol.) containing 0.3 wt. % NH_4F as an electrolyte solution.

The deposition of electrolytic Li_3PO_4 was performed on nt-TiO_2 as either amorphous material (labeled as AD) or, after calcination, as a anatase material (labeled as ADC), using a current density of −3.75 mA cm^{-2} for 1 min. Electrolytic Li_3PO_4 films were deposited by an electrochemical procedure consisting of proton reduction with a subsequent local increase of pH in the vicinity of the substrate surface, hydrogen phosphate dissociation and Li_3PO_4 deposition on the surface of the cathode[13]. Optional thermal annealing at 500 °C was performed. The thickness and active mass of the anode was 8 μm and 0.935 mg cm^{-2} respectively[13].

HRTEM and SAED images were collected with a Tecnai F-20 device operating at 200 kV. The X-ray diffraction (XRD) patterns were recorded with a Siemens D5000 instrument utilizing Cu Kα radiation. The X-ray photoelectron spectroscopy (XPS) measurements were performed with a SPECS Phobios 150MCD instrument using a Mg Kα source (1253.6 eV) and a chamber pressure of 4×10^{-9} mbar.

Electrochemical characterization and cycling properties (discharge—charge) were performed using a three electrode configuration with a Biologic-VMP instrument. The full cells were assembled in a glovebox under an Ar atmosphere. A 9 mm diameter lithium disk was used as reference electrode, with Li_3PO_4—ntTiO_2-based films and Li_2CoPO_4F used as counter and working electrodes. The electrolyte solution was 1 M $LiPF_6$ (EC:DEC) embedded in Whatman glass fiber disks. The full cell was cycled at 1C, 2 C and 5 C rates (C = 0.3 mA cm^{-2}). The activation of the positive electrode (Li_2CoPO_4F) offers the possibility of achieving a remarkable reversible capacity for the full cell. In the present study, the activation step of the Li_2CoPO_4F consisted of two successive cycles of galvanostatic charging to 5.4 V, followed by discharging to 3.0 V, at a 100 mA g^{-1} current density and using metallic Li as a counter electrode. When designing the full battery, it is quite important to obtain an optimal balance of cathode and anode both in terms of weight and electrochemical properties. The calculation of the energy density of the battery only considered the specific capacity and the working potential ($E_{cathode} - E_{anode}$) of the full battery, without further consideration of the mass of the active materials, electrolyte and packing materials.

References

1. Amine, K., Tukamoto, H., Yasuda, H. & Fujita, Y. A new three-volt spinel $Li_{1+x}Mn_{1.5}Ni_{0.5}O_4$ for secondary lithium batteries. *J. Electrochem. Soc.* **143,** 1607–1613 (1996).
2. Kim, M. G. & Cho, J. Reversible and High-Capacity Nanostructured Electrode Materials for Li-Ion Batteries. *Adv. Funct. Mater.* **19,** 1497–1514 (2009).
3. Fey, G. T. K., Li, W. & Dahn, J. R. $LiNiVO_4$ - A 4.8 volt electrode material for lithium cells. *J. Electrochem. Soc.* **141,** 2279–2282 (1994).
4. Kraytsberg, A. & Ein-Eli, Y. Higher, Stronger, Better … A Review of 5 Volt Cathode Materials for Advanced Lithium-Ion Batteries. *Adv. Energy. Mater.* **2,** 922–939 (2012).
5. Amine, K., Yasuda, H. & Yamachi, M. Olivine $LiCoPO_4$ as 4.8 V electrode material for lithium batteries. *Electrochem. Solid-State Lett*. **3,** 178–179 (2000).
6. Okada, S., Ueno, M., Uebou, Y. & Yamaki J. I. Fluoride phosphate Li_2CoPO_4F as a high-voltage cathode in Li-ion batteries. *J. Power Sources* **146,** 565–569 (2005).
7. Ohzuku, T., Ueda, A. & Yamamoto, N. Zero-strain insertion material of $Li[Li_{1/3}Ti_{5/3}]O_4$ for rechargeable lithium cells. *J. Electrochem. Soc.* **142,** 1431–1435 (1995).
8. Sorensen, E. M., Barry, S. J., Jung, H. K., Rondinelli, J. R., Vaughey, J. T. & Poeppelmeier, K. R. Three-dimensionally ordered macroporous $Li_4Ti_5O_{12}$: Effect of wall structure on electrochemical properties. *Chem. Mater.* **18,** 482–489 (2006).
9. Bruce, P. G., Scrosati, B. & Tarascon, J. M. Nanomaterials for rechargeable lithium batteries. *Angew. Chem.-Int. Edit*. **47,** 2930–2946 (2008).
10. Ortiz, G. F., Hanzu, I., Djenizian, T., Lavela, P., Tirado, J. L. & Knauth, P. Alternative Li-Ion Battery Electrode Based on Self-Organized Titania Nanotubes. *Chem. Mater.* **21,** 63–67 (2009).
11. Wu, X., Gong, Z., Tan, S. & Yang, Y. Sol-gel synthesis of Li_2CoPO_4F/C nanocomposite as a high power cathode material for lithium ion batteries. *J. Power Sources* **220,** 122–129 (2012).
12. Reale, P., Panero, S., Scrosati, B., Garche, J., Wohlfahrt-Mehrens, M. & Wachtler, M. A safe, low-cost, and sustainable lithium-ion polymer battery. *J. Electrochem. Soc.* **151,** A2138–A2142 (2004).
13. López, M. C., Ortiz, G. F., González, J. R., Alcántara, R. & Tirado, J. L. Improving the Performance of Titania Nanotube Battery Materials by Surface Modification with Lithium Phosphate. *ACS Appl. Mater. Interfaces* **6,** 5669–5678 (2014).
14. Cabello, M., Ortiz, G. F., López, M. C., Lavela, P., Alcántara, R. & Tirado, J. L. Self-assembled $Li_4Ti_5O_{12}/TiO_2/Li_3PO_4$ for integrated Li-ion microbatteries *Electrochem. Commun.* **56,** 61–64 (2015).
15. Wu, X., Wang, S., Lin, X., Zhong, G., Gong, Z. & Yang, Y. Promoting long-term cycling performance of high-voltage Li_2CoPO_4F by the stabilization of electrode/electrolyte interface. *J. Mater. Chem. A*, **2,** 1006–1013 (2014).
16. Truong, Q. D., Devaraju, M. K., Ganbe, Y., Tomai, T. & Honma I. Structural Analysis and Electrochemical Performance of Li_2CoPO_4F Cathode Materials. *Electrochim. Acta* **127,** 245–251 (2014).
17. Hadermann, J., Abakumov, A. M., Turner, S., Hafideddine, Z., Khasanova, N. R., Antipov, E. V. & Tendeloo, G. V. Solving the Structure of Li Ion Battery Materials with Precession Electron Diffraction: Application to Li_2CoPO_4F. *Chem. Mater.* **23,** 3540–3545 (2011).
18. Takada, K., Inada, T., Kajiyama, A., Sasaki, H., Kondo, S., Watanabe, M., Murayama, M. & Kanno, R. Solid-state lithium battery with graphite anode. *Solid State Ionics* **158,** 269–274 (2003).
19. Seki, S., Kobayashi, Y., Miyashiro, H., Mita, Y. & Iwahori, T. Fabrication of high-voltage, high-capacity all-solid-state lithium polymer secondary batteries by application of the polymer electrolyte/inorganic electrolyte composite concept. *Chem. Mater.* **17,** 2041–2045 (2005).
20. Du, Y. A. & Holzwarth, N. A. W. Mechanisms of Li^+diffusion in crystalline gamma- and beta-Li_3PO_4 electrolytes from first principles. *Phys. Rev. B.* **76,** 174302 (2007).
21. Frayret, C., Masquelier, C., Villesuzanne, A., Morcrette, M. & Tarascon, J. M. Comparative Studies on the Phase Stability, Electronic Structure, and Topology of the Charge Density in the Li_3XO_4 (X = P, As, V) Lithium Orthosalt Polymorphs. *Chem. Mater.* **21,** 1861–1874 (2009).
22. Zemann J. Die kristallstruktur von lithiumphosphat, Li_3PO_4. *Acta Crystallogr*. **13,** 863–867 (1960).
23. Keffer, C., Mighell, A., Mauer, F., Swanson, H. & Block, S. Crystal structure of twinned low-temperature lithium phosphate. *Inorg. Chem*. **6,** 119–125 (1967).
24. Laumann, ,A. Boysen, H., Bremholm, M., Fehr, K. T., Hoelzel, M. & Holzapfel, M. Lithium Migration at High Temperatures in $Li_4Ti_5O_{12}$ Studied by Neutron Diffraction. *Chem. Mater.* **23,** 2753–2759 (2011).
25. Rezaee, M., Khoie, S. M. M. & Liu, K. H. The role of brookite in mechanical activation of anatase-to-rutile transformation of nanocrystalline TiO_2: An XRD and Raman spectroscopy investigation. *CrystEngComm*, **13,** 5055–5061 (2011).
26. Bondareva O. S., Simonov M. A. & Belov N. V. The crystal structure of the synthetic analogue of the lithiophospate gamma-Li_3PO_4. *Doklady Akademii Nauk SSSR* **240,** 75–77 (1978).

27. Wang, D., Xiao, J., Xu, W., Nie, Z., Wang, C., Graff, G. & Zhang, J. G. Preparation and electrochemical investigation of Li_2CoPO_4F cathode material for lithium-ion batteries. *J. Power Sources* **196,** 2241–2245 (2011).
28. Amaresh, S., Karthikeyan, K., Kim, K. J., Kim, M. C., Chung, K. Y., Cho, B. W. & Lee, Y. S. Facile synthesis of ZrO_2 coated Li_2CoPO_4F cathode materials for lithium secondary batteries with improved electrochemical properties. *J. Power Sources* **244,** 395–402 (2013).
29. Amaresh, S., Karthikeyan, K., Kim, K. J., An, J. Y., Cho, S. J., Chung, K. Y., Cho, B. W., Nam, K. W. & Lee Y. S. Metal Oxide Coated Lithium Cobalt Fluorophosphate Cathode Materials for Lithium Secondary Batteries-Effect of Aging and Temperature. *J. Nanosci. Nanotechnol.* **14,** 7545–7552 (2014).
30. Okumura, T., Shikano, M., Yamaguchi, Y. & Kobayashi, H. Structural Changes in Li_2CoPO_4F during Lithium-Ion Battery Reactions. *Chem. Mater.* **27,** 2839–2847 (2015).
31. Jung, H. G., Jang, M. W., Hassoun, J., Sun, Y. K. & Scrosati, B. A high-rate long-life $Li_4Ti_5O_{12}$ / $Li[Ni_{0.45}Co_{0.1}Mn_{1.45}]O_4$ lithium-ion battery. *Nat. Commun.* **2,** 516 (2011).
32. Swiderska-Mocek A. Application of quaternary polymer electrolyte based on ionic liquid in $LiFePO_4$/Li, $Li_4Ti_5O_{12}$/Li and $LiFePO_4$/$Li_4Ti_5O_{12}$ batteries. *Electrochim. Acta* **139,** 337–344 (2014).
33. Kim, J. W., Kim, D. H., Oh, D. Y., Lee, H., Kim, J. H., Lee, J. H. & Jung, Y. S. Surface chemistry of $LiNi_{0.5}Mn_{1.5}O_4$ particles coated by Al_2O_3 using atomic layer deposition for lithium-ion batteries. *J. Power Sources* **274,** 1254–1262 (2015).
34. Prosini, P. P., Cento, C. & Pozio, A. Lithium-ion batteries based on titanium oxide nanotubes and $LiFePO_4$. *J. Solid State Electrochem.* **18,** 795–804 (2014).
35. Hassoun, J., Bonaccorso, F., Agostini, M., Angelucci, M., Betti, M. G., Cingolani, R., Gemmi, M., Mariani, C., Panero, S., Pellegrini, V. & Scrosati, B. An Advanced Lithium-Ion Battery Based on a Graphene Anode and a Lithium Iron Phosphate Cathode. *Nano Lett.* **14,** 4901–4906 (2014).
36. Verrelli, R., Scrosati, B., Sun, Y. K. & Hassoun J. Stable, High Voltage $Li_{0.85}Ni_{0.46}Cu_{0.1}Mn_{1.49}O_4$ Spinel Cathode in a Lithium-Ion Battery Using a Conversion-Type CuO Anode. *ACS Appl. Mater. Interfaces*. **6,** 5206–5211 (2014).
37. Zaghib, K., Simoneau, M., Armand, M. & Gauthier, M. Electrochemical study of $Li_4Ti_5O_{12}$ as negative electrode for Li-ion polymer rechargeable batteries. *J. Power Sources* **81–82,** 300–305 (1999).
38. Ronci, F., Reale, P., Scrosati, B., Rossi Albertini, V., Perfietti, P., Di Michiel, M. & Merino, J. M. High-Resolution *In-Situ* Structural Measurements of the $Li_{4/3}Ti_{5/3}O_4$ "Zero-Strain" Insertion Material. *J. Phys. Chem. B* **106,** 3082–3086 (2002).
39. Aldon, L., Kubiak, P., Womes, M., Jumas, J. C., Olivier-Fourcade, J., Tirado, J. L. Corredor, J. I. & Pérez Vicente, C. Chemical and Electrochemical Li-Insertion into the $Li_4Ti_5O_{12}$ Spinel. *Chem. Mater.* **16,** 5721–5725 (2004).

Acknowledgements

The authors are grateful to MEC (MAT2011-22753) and Junta de Andalucía for financial support (FQM-7206 and FQM-288). G.F. Ortiz is indebted to the "Ramón y Cajal" program (RYC-2010-05596) and to MESC for a scholarship at Xiamen University. Y. Yang acknowledges funding from the National Natural Science Foundation of China (Grant No. 21233004).

Author Contributions

G.F.O., J.L.T. and Y.Y. proposed and designed the experiments. Y.L. synthesized and performed the electrochemistry of the Li_2CoPO_4F material. G.F.O., M.C. and M.C.L. fabricated the titania nanotubes and TiO_2/Li_3PO_4 electrodes. M.J.M. conducted the TEM and SAED measurements. M.C. and M.C.L. carried out the experiments of the full batteries in three electrodes. G.F.O. and J.L.T. and Y.Y. co-wrote the paper. All authors discussed the results and commented on the manuscript.

Additional Information

Supplementary information accompanies this paper at http://www.nature.com/srep

Competing financial interests: The authors declare no competing financial interests.

How to cite this article: Ortiz, G. F. *et al.* Enhancing the energy density of safer Li-ion batteries by combining high-voltage lithium cobalt fluorophosphate cathodes and nanostructured titania anodes. *Sci. Rep.* **6**, 20656; doi: 10.1038/srep20656 (2016).